

ICESat-2 Reveals Accelerated Global Glacier Mass Loss Except Alaska From 2019 to 2023

Yubin Fan^{ID}, Lanhua Luo, Chang-Qing Ke^{ID}, and Genyu Wang

Abstract—The estimation of the worldwide glacier mass balance between 2019 and 2023 was accomplished through the utilization of ICESat-2 ATL06 data by employing a quadratic surface model fitting approach. Glaciers have a mass change of -331.68 ± 59.07 Gt/yr during this four-year span, which can be equivalated to a sea level rise of 0.916 ± 0.163 mm/yr. Accelerated but contrasting patterns of glacier mass change have been observed, with an accelerated mass loss found in regions such as Svalbard, Russian Arctic, the High Mountain Asia, and the southern Andes. In contrast, Alaska exhibited a decelerated mass loss, and some Antarctic glaciers experienced a slight mass gain. In the maritime regions, land-terminating glaciers have experienced more extensive mass loss except Svalbard and the Russian Arctic. The analysis of seasonal glacier changes indicated that the majority of regions demonstrated their lowest glacier mass in the summer of 2022, and lost approximately 50% mass during 2022–2023. These results provide valuable reference data for the assessment of glacier mass balance using ICESat-2.

Index Terms—Glacier mass balance, ICESat-2, quadratic surface fit, seasonal glacier change.

I. INTRODUCTION

GLACIERS distinct from the Greenland and Antarctic ice sheet cover an area of 706 000 km² [1], with an estimated glacier volume of $158 \pm 41 \times 10^3$ km³ [2]. Retreat and thinning of them due to global warming have led to local hazards and changed global energy cycles [3]. To understand and quantify changes in glacier mass (glacier mass balance), four main methods are commonly used: glaciological, digital elevation model (DEM) differencing, altimetry, and gravimetry.

Glaciological in-situ measurements rely on annual point mass balances obtained from stakes inserted in ice and from cores drilled in firn, but they can only cover a small portion of the global glaciers [4], they are unevenly distributed globally but can provide accurate seasonal and annual glacier mass changes,

Received 3 August 2024; revised 11 November 2024; accepted 11 December 2024. Date of publication 16 December 2024; date of current version 27 December 2024. This work was supported in part by the Science and Technology Plan Project of Jiangsu Province under Grant BZ2024032, and in part by Chizhou University High-level Talent Research Start-up Fund under Grant CZ2024YJRC12. (Corresponding author: Chang-Qing Ke.)

Yubin Fan is with the School of Geography and Planning, Chizhou University, Chizhou 247100, China (e-mail: 15850788815@163.com).

Lanhua Luo, Chang-Qing Ke, and Genyu Wang are with the Jiangsu Provincial Key Laboratory of Geographic Information Science and Technology, Key Laboratory for Land Satellite Remote Sensing Applications of Ministry of Natural Resources, School of Geography and Ocean Science, Nanjing University, Nanjing 210093, China (e-mail: orchid0918@163.com; kecq@nju.edu.cn; cherishwgy@163.com).

Digital Object Identifier 10.1109/JSTARS.2024.3518480

but the regional mass extrapolation of them may introduce significant biases for data sparsity. Understanding of glacier mass balance has been improved due to more frequent and larger-scale observations obtained by remote sensing datasets. Repeat observations from optical and radar DEMs can obtain detailed glacier elevation at high temporal and spatial resolution [5], [6]. Similarly, altimeters (both optical and radar) provide elevation along their tracks at different temporal resolutions [7], [8], and the interpolation of them can realize regional glacier elevation and volume change estimations. Both DEM differencing and altimeter-based methods require glacier density to convert glacier volume to mass changes. Gravity from Gravity Recovery and Climate Experiment (GRACE) and GRACE-Follow On (GRACE/FO) satellites can realize global observations [9], [10], and glacier mass changes can be measured by measuring variations in the gravitational field, but it suffers from the coarse leakage effects [11] and the complexity of signal source [12], thus the gravimetric results for regions with small glacier covers have no to low confidence due to implausible trends and variabilities.

Global estimates of glacier mass balance are still challenging. While there is a general agreement between different methods, there are considerable disparities in regional assessments and temporal trends of glacier loss. IPCC's sixth assessment report (AR6) finally complemented glaciological observations with global glacier mass balance from DEM differencing, using results from gravimetry for evaluation, and calculated their mean mass-change rates over 2000–2019 [13], but only a few studies have detected glacier mass over recent years [14], [15], [16]. Increased number of footprints and improved accuracy [17], [18] of ICESat-2 may favor the detection of mid-latitude glaciers in more detailed spatial scales [7], [19]. Seasonal glacier mass change provides insights into short-term fluctuations in glacier dynamics and hydrological processes, but global seasonal glacier mass data are lacking. The 91-day cycle of ICESat-2 also reveals the seasonal glacier change, which has been applied to reveal three glacial seasonal cycle regimes in High Mountain Asia (HMA) [20] and the seasonal glacier mass change in Karakoram during 2019–2022 [14].

Therefore, it is desirable to use ICESat-2 data collected from 2019 to 2023 to study the spatiotemporal glacier mass variations over this four-year period globally. To this end, we will:

- 1) estimate annual rates of glacier elevation change and mass balance by fitting a quadratic surface model to all ICESat-2 elevation measurements within 500 m grids;
- 2) obtain the seasonal glacier mass balance from 2019 to 2023 by comparing ICESat-2 with DEMs;

- 3) verify the glacier mass balance estimation by comparing it with ATL15 products and previous studies.

II. DATA

A. ICESat-2 Data

The ICESat-2 ATL06 product provides geolocated land surface height along the ground track with high horizontal and vertical accuracy and spaced 20 m apart [21]. This product includes correction parameters for instrument bias as an accompanying field. We used the ICESat-2 ATL06 product (version 6) spanning from March 2019 to March 2023 to assess glacier mass balance over this four-year period.

In addition, the ICESat-2 ATL15 product provides height-change maps for both Antarctic and Arctic land ice at three-month intervals from March 2019 to March 2022. This product offers varying resolutions that aid in detecting height change patterns and calculating integrated regional volume change. We used this data to cross-verify our glacier mass balance estimations. Both data are available through the National Snow and Ice Data Center.

B. DEM Data

NASADEM is an enhanced version of the SRTM DEM and has the best performance among the open-access DEMs in the mid-latitude regions [22], and it was used as a benchmark DEM outside polar regions.

ArcticDEM and REMA mosaic products are constructed by compiling from the highest-quality strip DEM files, which are blended and feathered to minimize gaps and the presence of artifacts at the edges. Filtered ICESat altimetry data has been incorporated to enhance their overall accuracy. ArcticDEM and REMA v4.1 mosaic DEMs of 500 m resolution were used as the benchmark DEM in the polar regions.

C. Glacier Regions and Glacier Area

We utilized the 19 first-order glacier regions as delineated by the Global Terrestrial Network for Glaciers [1]. These 19 regions are deemed suitable for mass-balance studies due to their manageable number and geographical extent, excluding those that cover the ice sheet peripheries. The regions are Alaska (ALA), Western Canada and USA (WCU), Arctic Canada North (ACN), Arctic Canada South (ACS), Greenland periphery (GP), Iceland (IC), Svalbard and Jan Mayen (SV), Scandinavia (SC), Russian Arctic (RA), North Asia (NA), Central Europe (CE), Caucasus and Middle East (CM), Central Asia (CA), South Asia West (SAW), South Asia East (SAE), Low Latitudes (LL), Southern Andes (SA), New Zealand (NZ), and Antarctic and Subantarctic (ANT). In the following text, we will assign them numbers 1–19.

Regional glacier areas were aggregated from the Randolph Glacier Inventory (RGI 6.0), which provides an inventory with a digital outline and area for each glacier globally, approximately around the year 2000. For these regional glacier areas, we estimate a general uncertainty of $\pm 10\%$ [19] to account for potential changes in regional glacier areas.

TABLE I
QUALITY CONTROL CRITERIA APPLIED TO REMOVE THE UNREALISTIC VALUES DUE TO THE POOR FITTING PERFORMANCES IN EACH GRID

Parameters	Values
Elevation change rate	$\geq \pm 15 \text{ m/yr}$
Uncertainty of elevation change rate	$\geq 15 \text{ m/yr}$
Time span	≤ 2
Number of ICESat-2 measurements	≤ 15
Difference between benchmark DEM	$\geq \pm 200 \text{ m}$

III. METHODS

A. Rates of Elevation Change and Uncertainty

To compute elevation-change rate, ICESat-2 elevation measurements were separated into $500 \text{ m} \times 500 \text{ m}$ grid, then a model fit method was used to separate the various contributions to the measured elevation fluctuations [23]. We determine the elevation (h_i) as a quadratic surface of local surface terrain using an iterative least-squares fitting approach (1), and a linear rate of elevation change with time

$$h_i = h + a_0x + a_1y + a_2x^2 + a_3y^2 + a_4xy + \frac{dh}{dt}(t - t_{\text{mid}}). \quad (1)$$

This model accounts for surface elevation variations through parameters a_0 , a_1 , a_2 , a_3 , and a_4 , which were estimated by an iterative least-squares fitting approach. The rate of elevation change (dh/dt) is calculated by examining the elevation changes over time relative to a midpoint timestamp (March 2021). For the coordinate systems, UTM projections were used for low to mid-latitudes, while polar stereographic projections were applied in polar regions.

The uncertainty of elevation change rate in each grid was calculated by the following.

$$\sigma_{h_i} = t(1 - 0.025, n-p) \times \text{SE}(b_i) \quad (2)$$

where b_i represents the elevation change rate, $\text{SE}(b_i)$ is the standard error of the elevation change rate, and $t(1-0.025, n-p)$ is the 95% percentile of t -distribution with $n-p$ degrees of freedom, n is the number of ICESat-2 measurements within one grid, p denotes the number of regression coefficients, which is 7 in this case.

To address the possibility of inadequate fits within specific grids, we implemented quality control focusing on data availability and rationality (see Table I). This involved assessing the number of ICESat-2 measurement points, the temporal range of the data utilized, the accuracy of fitted elevations, and the uncertainty elevation change rates associated with its uncertainty. Elevation-change uncertainties across grids are assumed to be fully correlated within a given geographical region, therefore when transitioning from grid-level uncertainties (σ_{h_i}) to regional uncertainties (σ_{dh}), it is crucial to consider the decorrelation distance (L). To estimate the decorrelation distance, a semivariogram cloud with a lag distance of 10 km was employed for each region. Based on this estimated decorrelation distance, the effective sample size (N_{eff}) was then calculated [8], [24], and

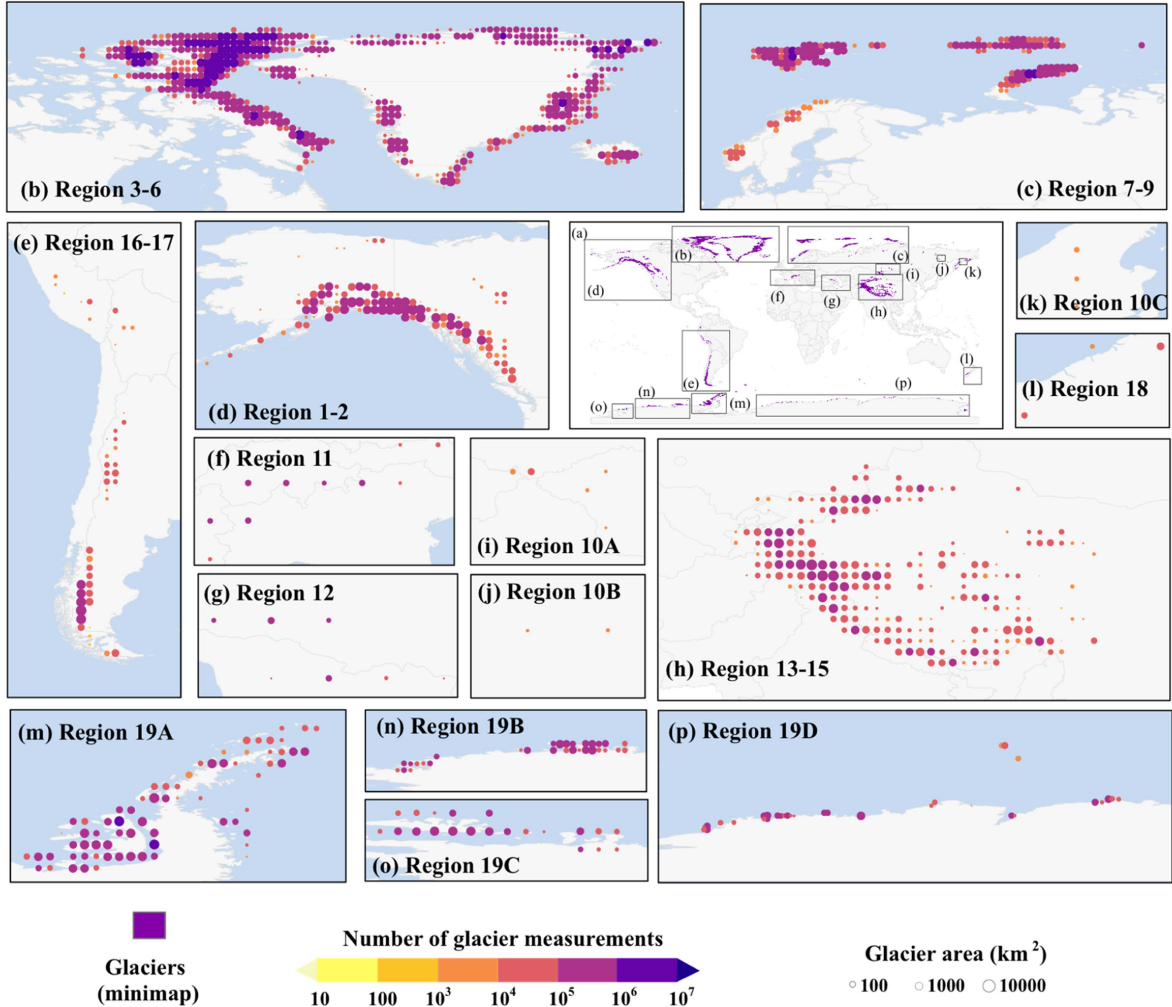


Fig. 1. Number of glacier measurements for the period from 2019 to 2023. Data are shown on a $1^\circ \times 1^\circ$ grid. The circle color represents the number variation, and the circle size is scaled according to the glacier area.

the regional elevation uncertainty was derived by (4)

$$N_{\text{eff}} = \frac{N_{\text{total}} r^2}{L^2} \quad (3)$$

where N_{total} is the number of calculated pixels in region of interest, L is the decorrelation distance, and r is the grid size (500 m)

$$\sigma_{dh} = \frac{\sqrt{\sum_{i=1}^n \sigma_{h_i}^2}}{N_{\text{eff}}} \quad (4)$$

B. Mass Balance Estimation and Uncertainty

It is crucial to ensure that the ICESat-2 samples matched the glacier hypsometry accurately to attain a statistically reliable signal. However, hypsometry often presents disparities in smaller areas of interest, like $1^\circ \times 1^\circ$ grids. To address this, an iterative approach was adopted, gradually adjusting the ICESat-2 footprints to better align with the glacier hypsometry provided by the benchmark DEM, using a 100-m elevation interval. This process was conducted within 500 m grids, resulting in estimates of elevation change and mass change from the reduced

samples. Grids showing large hypsometry differences between the benchmark DEM and ICESat-2 data were excluded from further analysis.

For the mid-latitude region, given that the data coverage is relatively lower ($\sim 30\%-40\%$) (see Figs. 1 and 2), but is able to sample the full hypsometry range except for regions composed of small and widely scattered glacier covers. To address missing data, we applied interpolation methods under the assumption that glaciers within the same elevation bin exhibit similar rates of elevation change. We then divided each subregion into elevation zones with 100 m intervals and computed the mean elevation change (E_i) for each zone. Volume change was subsequently determined by multiplying E_i by the glacier area (A_i) corresponding to each zone. Using an ice density of 850 kg/m^3 , volume change was converted into mass change, ultimately deriving the final mass balance change (dB) using the following equation [25]:

$$dB = \frac{\rho_{\text{ice}}}{A_{\text{total}} * \rho_{\text{water}}} \sum_{k=1}^n A_i * E_i \quad (5)$$

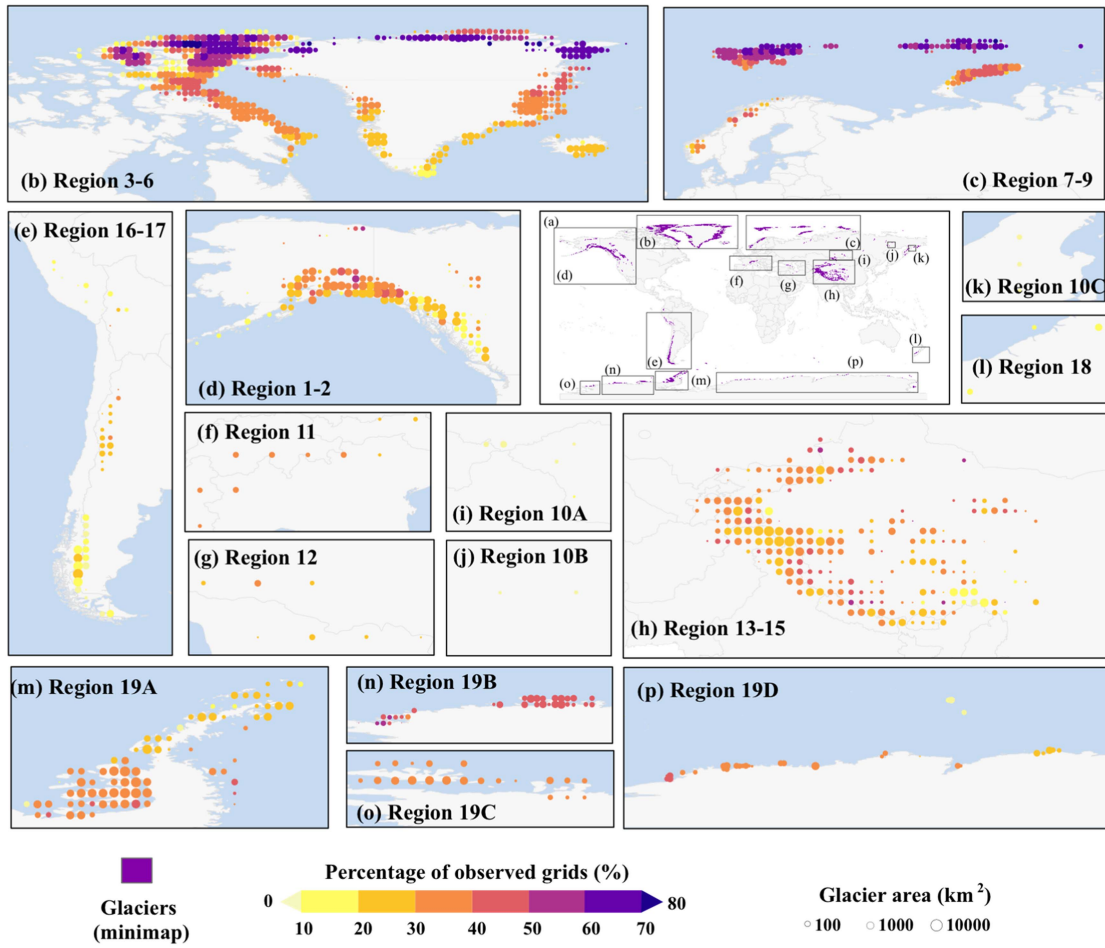


Fig. 2. Data coverage for the period from 2019 to 2023. Data are shown on a $1^\circ \times 1^\circ$ grid as described in Fig. 1. Coverage is displayed as the percentage (%) of observed areas of elevation change maps within each $1^\circ \times 1^\circ$ grid relative to the glacier area. The circle size is scaled according to the glacier area.

where n is the number of elevation zones, ρ_{ice} is the glacier ice density, ρ_{water} is the mass density of water (1000 kg/m^3), and A_{total} is the total glacier area in each subregion.

The uncertainties associated with regional mass are impacted by the uncertainty in glacier area, σ_A ($\pm 10\%$), and the uncertainty in glacier density, σ_{ice} ($\pm 60 \text{ kg/m}^3$). The uncertainty of glacier volume (σ_V) and mass changes (σ_B) will be estimated as follows:

$$\sigma_V = \sqrt{(\sigma_h * A)^2 + (\sigma_A * dh)^2} \quad (6)$$

$$\sigma_B = \sqrt{\left(\frac{\rho_{\text{ice}}}{\rho_w * A} * \sigma_V \right)^2 + \left(\frac{V}{\rho_w * A} * \sigma_{\text{ice}} \right)^2} \quad (7)$$

where σ_V is the uncertainty in glacier volume, σ_h is the uncertainty in elevation changes, A is the glacier area, σ_A is the uncertainty of glacier area, dh is the mean value of glacier elevation-change rate, σ_B is the uncertainty in mass change, ρ_{ice} is the mean ice density (850 kg/m^3), ρ_w is the water density, V and σ_V are the glacier volume change and its uncertainty, respectively.

C. Monthly Glacier Mass Changes

In addition to model fit, monthly elevation time-series were produced for all RGI regions using a 90-day moving window. Within each subregion, we determined the relative elevation change for all glaciers between ICESat-2 and the benchmark DEM within each 100-m elevation bin, and the region-wide glacier change was determined by aggregating the area-weighted relative elevation change values across all elevation bins. We computed the cumulative volume change and its associated uncertainty in the same manner as previously described. The detailed flow chart of this study can be seen in Fig. 3.

IV. RESULTS

A. Altitudinal Distribution of Glacier Elevation Changes

The altitudinal distributions of glacier elevation changes across 19 subregions are shown in Fig. 4. The common pattern of decreasing rates in glacier elevation with increasing altitude can be observed. Substantial mass loss is evident across elevation bins in nearly all regions, even at the highest elevations. Notably, glaciers in New Zealand showed positive elevation changes above 1500 m, while glaciers in the Antarctic periphery

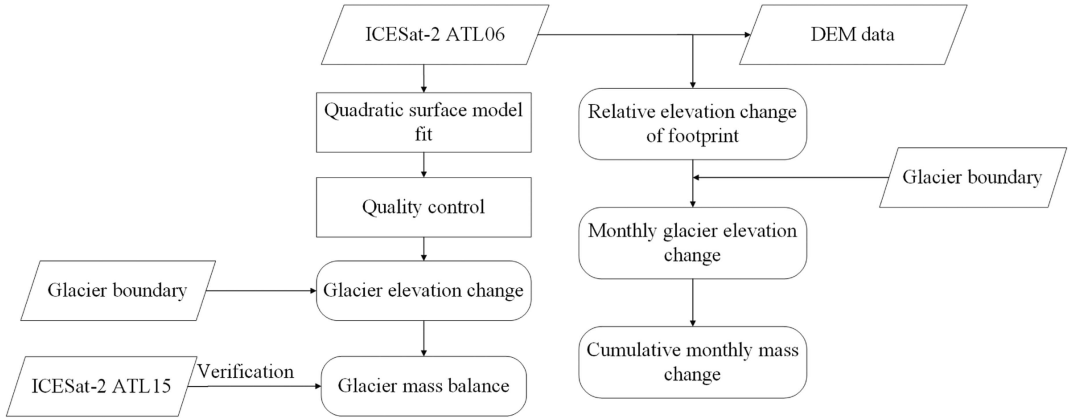


Fig. 3. Flowchart of this study.

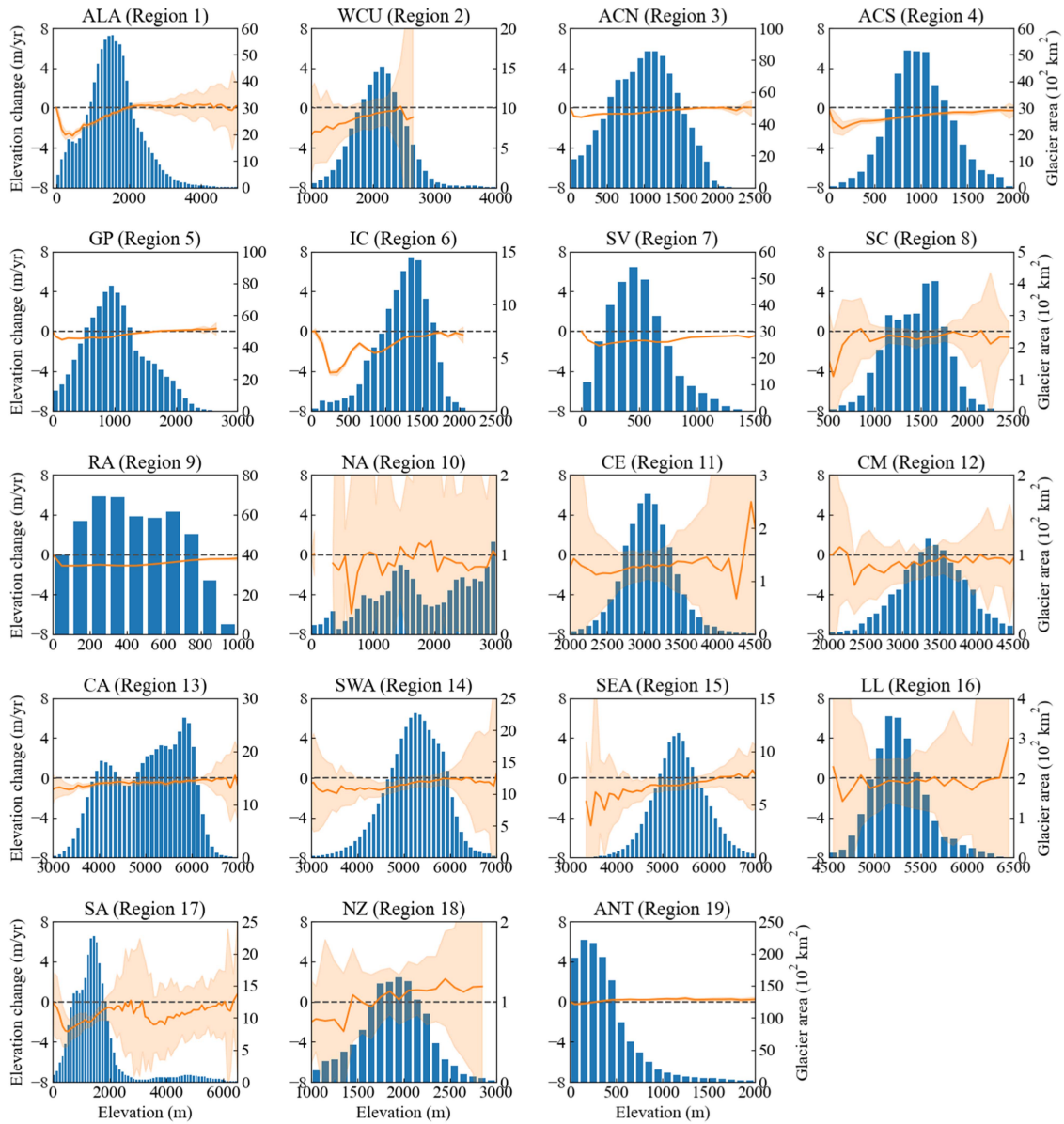


Fig. 4. Altitudinal distribution of glacier elevation changes in 19 subregions. The orange lines represent the elevation change rates with uncertainty envelopes for each 100 m elevation bin (left y-axis). The horizontal lines indicate a zero line to the elevation change. The bars of each subplot display the glacier area of the corresponding bin (right y-axis).

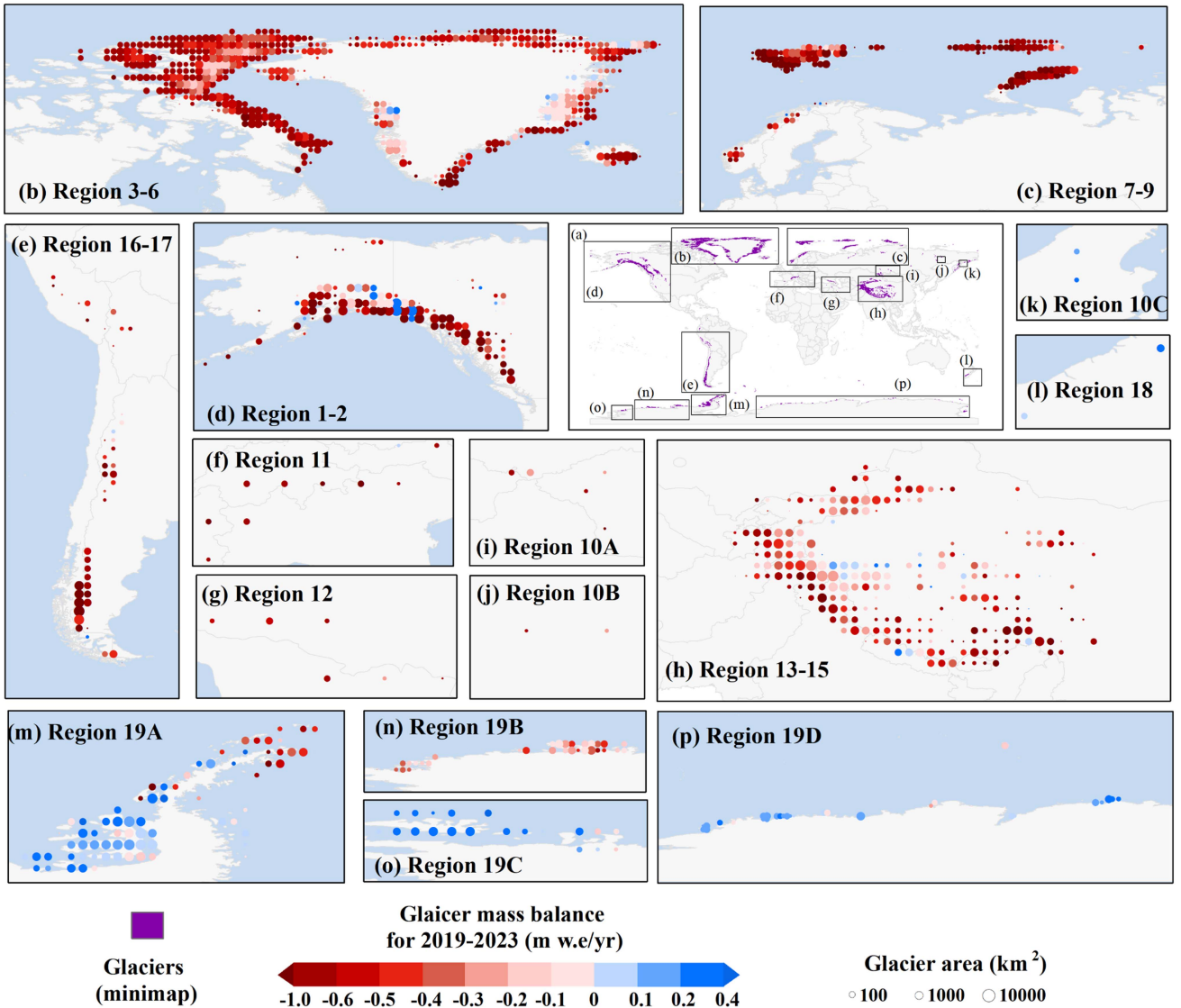


Fig. 5. Glacier mass balance changes for the period from 2019 to 2023. Data are shown on a $1^\circ \times 1^\circ$ grid. The circle color represents the mass balance variation, and the circle size is scaled according to the glacier area. Grids that do not match the glacier hypsometry were eliminated. 10A: Altay and Sayan, 10B: Chersky and Sunart Khayata, 10C: NE Russia, 19A: Antarctic peninsula, 19B: Marie Byrd Land, 19C: Ross Ice Shelf, and 19D: East Antarctic.

remained stable across all elevation bins. The increased uncertainty at low/high altitudes can be attributed to limited data collected in small-glaciated areas or steep slopes. In addition, small-glaciated regions including Western Canada and USA, Scandinavia, North Asia, Central Europe, Caucasus and Middle East, Low Latitudes, and New Zealand exhibit larger elevation-change uncertainties, collectively accounting for 3.8% of the total global glacier area, which has a relatively minor impact on the estimation of global glacier mass balance estimation.

B. Contrasting Regional Patterns of Glacier Mass Balance

A global glacier mass loss of approximately -331.68 ± 59.07 Gt/yr was estimated from 2019 to 2023, which can be equivalated to a sea level rise of 0.916 ± 0.163 mm/yr. Fig. 5 shows the glacier mass changes aggregated over $1^\circ \times 1^\circ$ grids in detail, revealing a widespread negative glacier mass balance

on a global scale. The specific mass change exhibited significant variation with latitude, and the northeastern Canadian Arctic and northern Svalbard experienced a moderate mass loss of approximately -0.3 m w.e./yr. Conversely, the southern Canadian Arctic, Alaska, and the southern Greenland Periphery consistently displayed more negative specific-mass change rates, indicating a relatively substantial thinning rate of up to -1 m w.e./yr. Middle latitude regions, such as Karakoram and eastern Kun Lun Shan, demonstrated a lower glacier mass loss rate of approximately -0.2 m w.e./yr. In contrast, some regions exhibited a positive balance over these 4 years, notably in northeast Russia, New Zealand, the northern Kun Lun Shan in the HMA, and the Antarctic periphery excluding the Marie Byrd Land.

Surface elevation change maps can be found in Fig. 6. Mass changes across various regions exhibited significant variability, predominantly characterized by a decline in glacier mass in most subregions (see Fig. 7 and Table II). Notably,

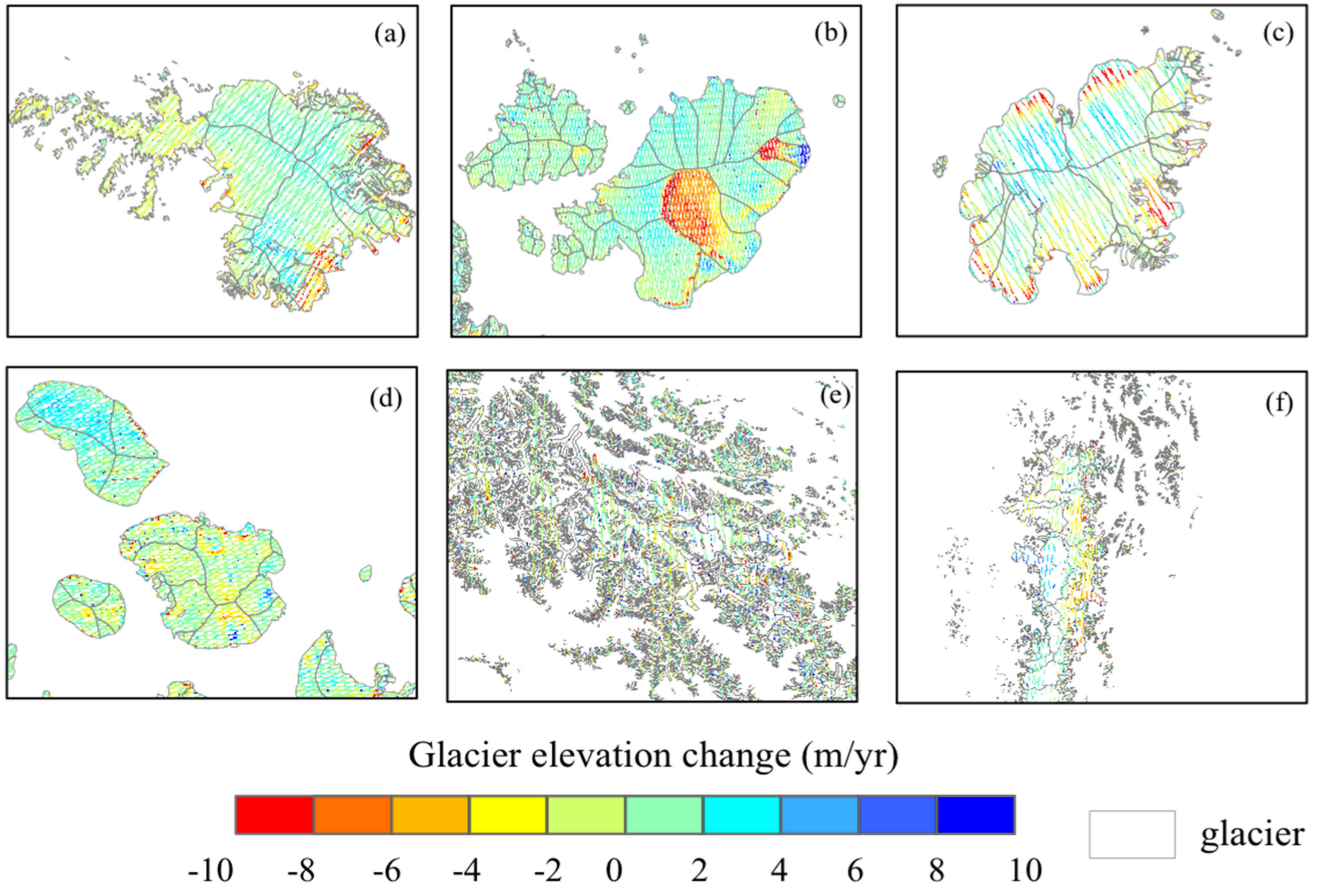


Fig. 6. Elevation changes during 2019–2023 over various regions. (a) Daven Island, Arctic Canada North. (b) Svalbard. (c) Iceland. (d) Severnaya Zemlya, Russian Arctic. (e) Karakoram. (f) Patagonia, Southern Andes.

TABLE II
REGIONAL RATES OF GLACIER MASS CHANGE BETWEEN 2019 AND 2023

Region	Mass balance (m w.e/yr)	Mass balance (Gt/yr)	SLE contribution (mm/yr)	Percentage of land-terminating contribution (%)
1 Alaska	-0.64±0.09	-57.11±7.68	-0.158±0.021	62.96
2 Western Canada and USA	-0.6±0.40	-8.34±5.52	-0.023±0.015	100
3 Arctic Canada North	-0.36±0.04	-36.24±4.45	-0.100±0.012	61.54
4 Arctic Canada South	-0.66±0.09	-27.16±3.57	-0.075±0.010	93.76
5 Greenland periphery	-0.36±0.04	-31.72±3.92	-0.088±0.011	61.60
6 Iceland	-0.84±0.10	-9.63±1.19	-0.027±0.003	100
7 Svalbard and Jan Mayen	-0.86±0.11	-28.14±3.44	-0.078±0.010	47.06
8 Scandinavia	-0.46±0.23	-1.39±0.70	-0.004±0.002	100
9 Russian Arctic	-0.8±0.10	-44.37±5.44	-0.123±0.015	26.91
10 North Asia	-0.42±1.38	-0.98±3.24	-0.003±0.009	100
11 Central Europe	-1.00±0.47	-2.10±0.97	-0.006±0.003	100
12 Caucasus and Middle East	-0.61±0.39	-0.77±0.49	-0.002±0.001	100
13 Central Asia	-0.40±0.07	-19.77±3.49	-0.055±0.010	100
14 South Asia West	-0.46±0.09	-15.59±3.12	-0.043±0.009	100
15 South Asia East	-0.54±0.13	-7.90±1.87	-0.022±0.005	100
16 Low Latitudes	-0.38±0.90	-0.89±2.09	-0.002±0.006	100
17 Southern Andes	-1.39±0.22	-40.84±6.41	-0.113±0.018	31.45
18 New Zealand	0.32±0.72	0.37±0.83		100
19 Antarctic and Subantarctic	0.007±0.005	0.89±0.64		

Note: In Greenland, glaciers highly connected to the ice sheet (RGI 6.0 connectivity level 2) are not reported.

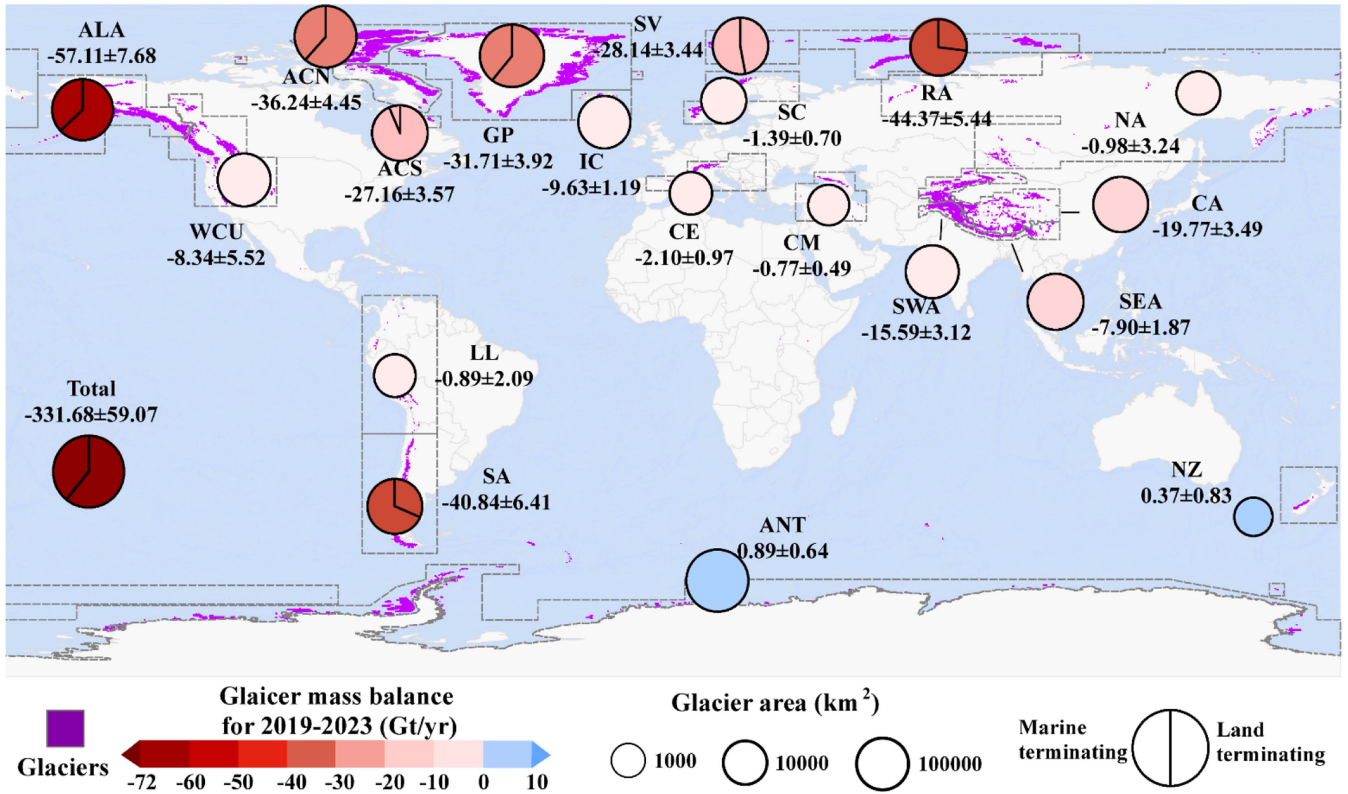


Fig. 7. Regional glacier mass changes for the period from 2019 to 2023 aggregated over the 19 RGI 6.0 regions (black-dotted polygons). The circle color represents the mass balance variation, and the circle size is scaled according to the glacier area. Pie chart shows the proportion of mass change contribution of marine-terminating and land-terminating glaciers relative to the total mass change, and the upper left section represents marine-terminating glaciers.

TABLE III
REGIONAL RATES OF LAND- AND MARINE-TERMINATING GLACIERS IN MARITIME REGIONS BETWEEN 2019 AND 2023

Region	Mass balance (m w.e./yr)		Mass balance (Gt/yr)	
	Land-terminating	Marine-terminating	Land-terminating	Marine-terminating
1 Alaska	-0.64 ± 0.09	-57.11 ± 7.68	-0.158 ± 0.021	62.96
2 Western Canada and USA	-0.60 ± 0.40	-8.34 ± 5.52	-0.023 ± 0.015	100
3 Arctic Canada North	-0.36 ± 0.04	-36.24 ± 4.45	-0.100 ± 0.012	61.54
4 Arctic Canada South	-0.66 ± 0.09	-27.16 ± 3.57	-0.075 ± 0.010	93.76
5 Greenland periphery	-0.36 ± 0.04	-31.72 ± 3.92	-0.088 ± 0.011	61.60
6 Iceland	-0.84 ± 0.10	-9.63 ± 1.19	-0.027 ± 0.003	100
7 Svalbard and Jan Mayen	-0.86 ± 0.11	-28.14 ± 3.44	-0.078 ± 0.010	47.06
8 Scandinavia	-0.46 ± 0.23	-1.39 ± 0.70	-0.004 ± 0.002	100
9 Russian Arctic	-0.80 ± 0.10	-44.37 ± 5.44	-0.123 ± 0.015	26.91

Note: In Greenland, glaciers highly connected to the ice sheet (RGI 6.0 connectivity level 2) are not reported.

Alaska emerged as the foremost contributor to global glacier mass change, with a substantial mass balance loss of approximately -57.11 ± 7.68 Gt/yr, which corresponds to approximately 16.57% of the global mass loss (see Fig. 7 and Table II). Both the northern and Canadian Arctic South showed extensive mass losses, amounting to -36.24 ± 4.45 Gt/yr and -27.16 ± 3.57 Gt/yr, respectively. The Greenland periphery and the Russian Arctic account for a large percentage of the global mass loss (~22.94%), followed by Svalbard with a glacier mass loss of -28.14 ± 3.44 Gt/yr. In the mid-latitude regions, the HMA and the southern Andes displayed the most significant glacier losses. Even smaller glaciated areas such as Central Europe and Scandinavia exhibited mass losses, albeit

contributing relatively less to the global mass change. However, it is important to note that despite covering the largest glacier area, the Antarctic peripheral glaciers demonstrated a mass balance. Notably, New Zealand and the Antarctic periphery exhibited positive anomalies, indicating a combined total mass gain of 1.26 Gt/yr, but remains comparatively small when contrasted with the overall mass loss.

Land-terminating glaciers represent 56% of the total glacier area and contribute to approximately 60% of global glacier mass loss, while marine-terminating glaciers account for around 40% (see Table III). In most regions, land-terminating glaciers have experienced more extensive mass loss compared to their

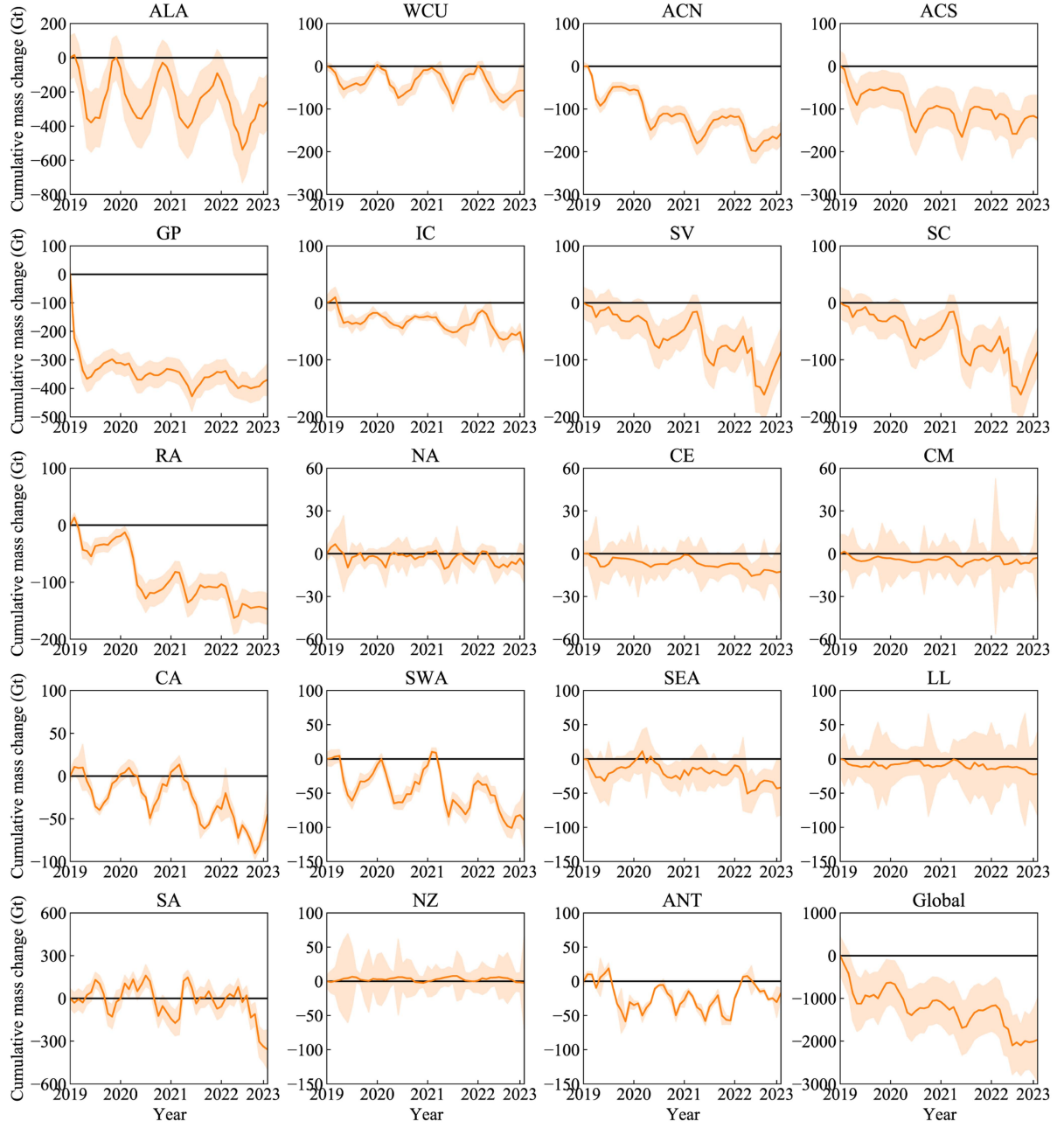


Fig. 8. Time-dependent glacier mass changes for each subregion. The orange line displays a cumulative monthly mass change in Gigatonnes [Gt] with its uncertainty.

marine-terminating counterparts, with the exception of Svalbard and the Russian Arctic. The delayed and asynchronous response of tidewater glaciers to climate changes may partly explain why most marine-terminating glaciers exhibit reduced mass [26], [27].

C. Seasonal Cycles of Glacier Mass

The monthly cumulative mass change revealed clear seasonal cycles across 19 subregions (see Fig. 8). In the Northern Hemisphere, most glaciers thicken during winter and spring and become thinner in summer and autumn, typically reaching their lowest values in September or October. Some

regions, such as Alaska, Western Canada, and the USA, showed stable glacier mass in 2019 and 2020 but experienced noticeable negative mass balances in 2021 and 2022. Additionally, Arctic Canada North demonstrated a consistent declining trend over the four-year period. Despite these variations, the majority of regions in the Northern Hemisphere recorded their lowest glacier mass in the summer of 2022. This significant decline can be attributed to the unprecedented heatwaves that affected Eurasia, North America, and China in 2022. These extreme temperatures led to exceptional glacier mass losses, as corroborated by studies on Swiss glaciers [28] and Urumqi Glacier No. 1 [29], which further support our findings.

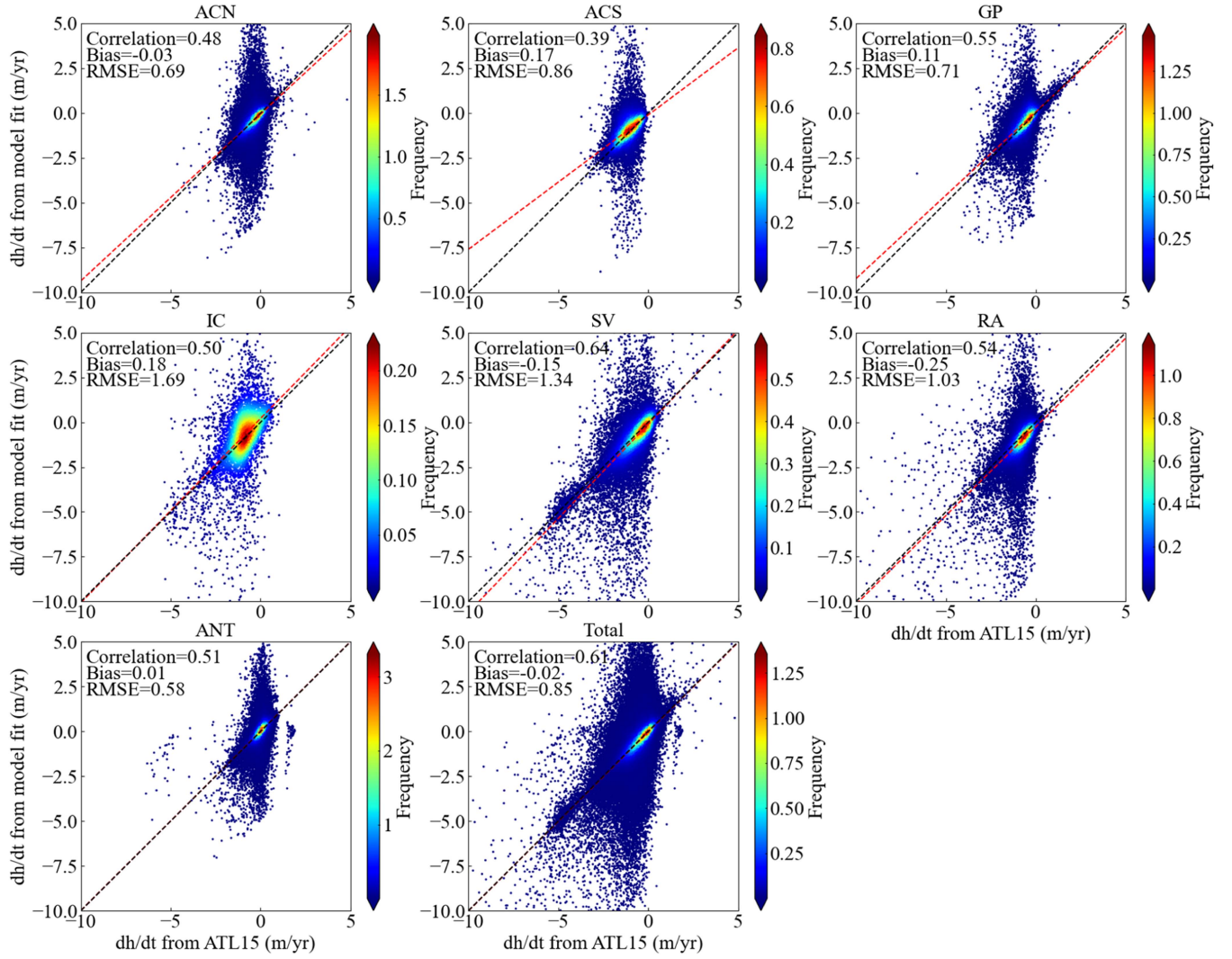


Fig. 9. Density scatter plot between glacier elevation change rates derived from ATL15 and model fit using Gaussian kernels for estimate of the probability density function in various regions. (a) Arctic Canada North. (b) Arctic Canada South. (c) Greenland periphery. (d) Iceland. (e) Svalbard and Jan Mayen. (f) Russian Arctic. (g) Antarctic and Subantarctic. (h) All regions covered by ATL15. The red dotted lines represent the linear regression fits, while the statistics provided in the top left corner of each panel offer various metrics for comparison.

In contrast, glaciers in the Southern Hemisphere exhibited a different accumulation pattern. Glaciers in the low latitudes and the Southern Andes showed minimal changes before 2022 but began to experience significant mass loss in 2022. Glaciers in New Zealand displayed only seasonal fluctuations without notable mass loss. Meanwhile, glaciers in the Antarctic periphery experienced a decline from 2019 to 2022 but rebounded to near-zero levels during 2022–2023.

V. DISCUSSIONS

A. Comparison With Previous Studies

Comparing our glacier mass balance calculations with existing data is crucial for verifying their precision and reliability. Initially, we compared our results with the ICESat-2 ATL15 product, which also assesses glacier mass balance in polar regions over a similar timeframe. We performed model fitting for the period 2019–2022 at a 1 km resolution to determine surface

elevation change rates, allowing for a direct comparison with the ATL15 dataset.

The surface change rates derived from our model fitting cover a smaller area but show close agreement with the ATL15 data within the error bars (see Fig. 9). Generally, our model fitting results tend to overestimate mass loss in high-latitude regions and underestimate it in low-latitude regions. Minor discrepancies are seen in higher-latitude regions such as Greenland, Antarctic, and Arctic Canadian North, where the RMSE is less than 0.71 m/yr. However, significant discrepancies are noted in the low-latitude regions, particularly in the Iceland ice caps and Arctic Canada South. For the Iceland ice caps, the correlation coefficient drops to 0.50, and the RMSE is 1.69 m/yr. Similarly, for Arctic Canada South, the correlation coefficient is as low as 0.39, with an RMSE of 0.86. On a global scale, these biases are mitigated, with a correlation coefficient of 0.61 and an RMSE of 0.85 m/yr, and the bias reduced to -0.02 m/y. We attribute these deviations to differences in calculation methods. The ATL15 product is based

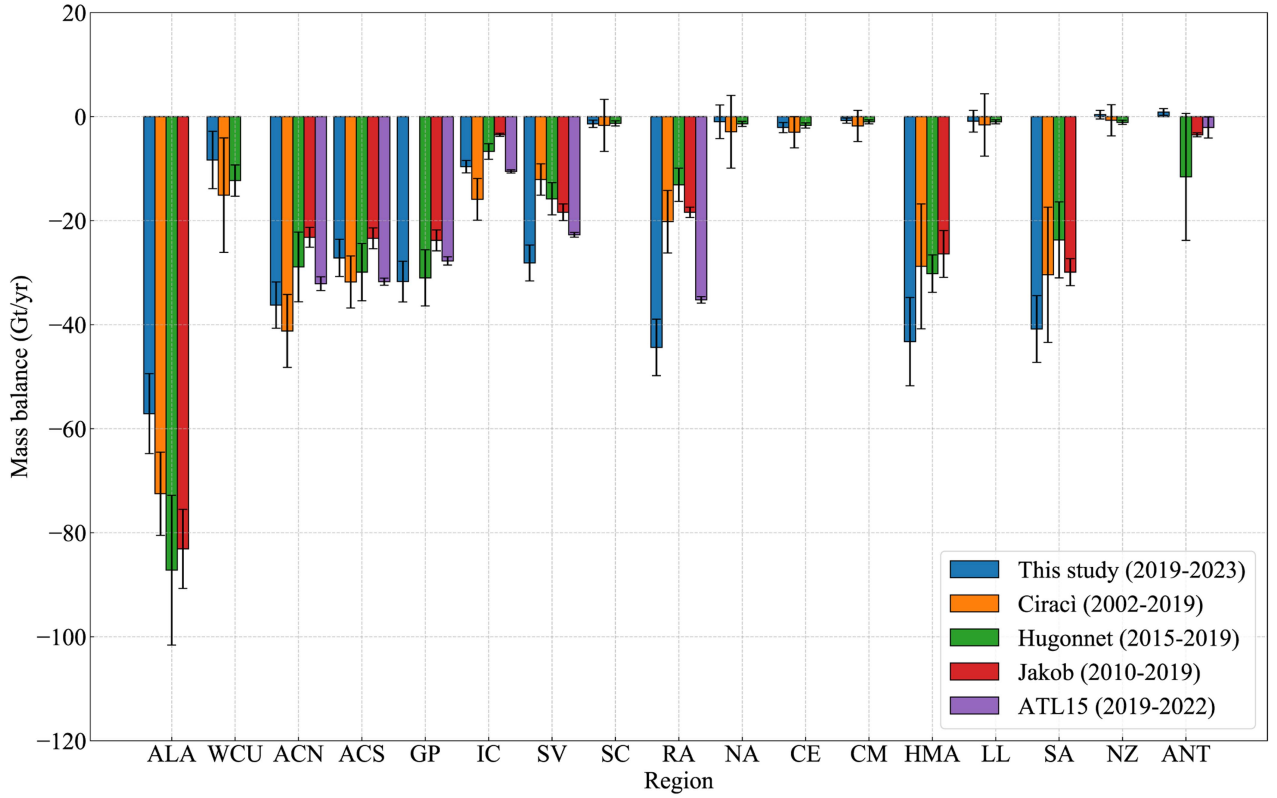


Fig. 10. Comparison of regional mass change estimates with earlier studies. We display a comparison of mass change estimate (Gt/yr) and its uncertainties at regional level. HMA includes Central Asia, South Asia West, and South Asia East. The time period is noted in the legend.

on gridding the ATL11 data, which uses a repeat-track method to provide land ice surface elevations with a 91-day cycle in polar regions by correcting offsets between the reference ground track and the ATL06 land ice measurements. In contrast, our model fitting directly estimates mass changes by integrating all ATL06 footprints within each grid.

While global estimates may vary due to differences in the study periods, our global estimate remains consistent with previous studies, falling within their error margins [6], [8], [9]. Our estimated mass balance of -331.68 ± 59.07 Gt/yr closely aligns with the -298 ± 24 Gt/yr reported for 2015–2019 [6], although our estimate is slightly higher, suggesting an accelerated global glacier mass loss. Regional comparisons are generally consistent with earlier studies but reveal some notable differences (see Fig. 10). Specifically, we observe larger mass losses in Svalbard, the Russian Arctic, and the HMA region. This indicates that these three regions are experiencing accelerated glacier mass loss compared to the 2000–2020 period, whereas Alaska's loss rate has slowed but remains the most severe globally.

B. Limitations and Future Perspectives

The study span is relatively short, which constrains long-term glacier change observations and makes it difficult to distinguish seasonal signals from interannual variations. For regions composed of small and widely scattered glaciers (such as North Asia and New Zealand), the uncertainty in elevation and volume changes is relatively high. The percentage of valid observed grids is low, posing challenges in obtaining reliable regional

elevation-change estimates. Improving monitoring accuracy for these areas is a key direction for future research.

However, the study shows that accurate mass balance monitoring can be achieved using only altimetry data. A promising direction for future research involves integrating data from other satellite missions, such as GEDI and Cryosat-2, to further enhance ICESat-2's monitoring capabilities and extend the spatial coverage of observed glaciers.

VI. CONCLUSION

We provide spatially and temporally resolved annual averaged estimates of mass changes for all glacier regions defined in the RGI using a quadratic surface model fitting approach and analyze monthly cumulative mass change by comparing them with benchmark DEMs. Our geodetic balance obtained from ICESat-2 using a quadratic surface model fitting approach provides the most recent global mass change update, showing that global glaciers experienced significant mass loss of -331.68 ± 59.07 Gt/yr from 2019 to 2023, with Alaska being the largest contributor to this change.

A common pattern of decreasing rates in glacier elevation with increasing altitude can be observed. Most regions have experienced an acceleration in mass loss, except for Alaska, where a deceleration in mass loss is observed, and New Zealand and the Antarctic periphery, where slight mass gain is noted. The seasonal variability of glacier mass change is also region-dependent, with most glaciers thickening in the winter and spring and becoming thinner in the summer and autumn in the

northern hemisphere. Most regions demonstrated their lowest glacier mass in the summer of 2022.

Our recent estimates of glacier mass loss using ICESat-2 confirm the magnitude of recent changes for the period from 2019 to 2023, aligning with global findings of accelerated mass loss. The consistency in both magnitude and uncertainty at this regional scale demonstrates that ICESat-2 can serve as a valuable complement to glacier mass balance studies, particularly with the impending discontinuation of ASTER. This study can enhance our understanding of glacier dynamics over extended temporal sequences, supporting the refinement of hydrological and glacier models essential for predicting regional and global water resources, sea level rise, and climate change impacts.

ACKNOWLEDGMENT

The authors would like to thank the anonymous reviewers for providing fruitful comments. The ICESat-2 data used in this study were obtained from the National Snow and Ice Data Center (<http://nsidc.org>). The NASADEM data were obtained from NASA (<https://search.earthdata.nasa.gov/>). ArcticDEM and REMA mosaic products can be available from <https://www.pgc.umn.edu/data/arcticdem/> and <https://www.pgc.umn.edu/data/remap/>. The glacier boundaries were obtained from http://www.glims.org/RGI/rgi60_dl.html.

REFERENCES

- [1] RGI Consortium, “Randolph glacier inventory – A dataset of global glacier outlines: Version 6.0,” distributed by Global Land Ice Measurements from Space, 2017. Accessed: Dec. 2023. [Online]. Available: <http://www.glims.org/RGI/>
- [2] D. Farinotti et al., “A consensus estimate for the ice thickness distribution of all glaciers on Earth,” *Nat. Geosci.*, vol. 12, no. 3, pp. 168–173, 2019.
- [3] W. W. Immerzeel, B. L. P. Van, and M. F. Bierkens, “Climate change will affect the Asian water towers,” *Science*, vol. 328, pp. 1382–1385, 2010.
- [4] M. Zemp et al., “Global glacier change bulletin No. 5 (2020–2021),” *WGMS*, 2023.
- [5] F. Brun, E. Berthier, P. Wagnon, A. Kääb, and D. Treichler, “A spatially resolved estimate of high mountain Asia glacier mass balances from 2000 to 2016,” *Nat. Geosci.*, vol. 10, pp. 668–673, 2017.
- [6] R. Hugonnet et al., “Accelerated global glacier mass loss in the early twenty-first century,” *Nature*, vol. 592, pp. 726–731, 2021.
- [7] C. Shen, L. Jia, and S. Ren, “Inter-and intra-annual glacier elevation change in high mountain Asia region based on ICESat-1&2 data using elevation-aspect bin analysis method,” *Remote Sens.*, vol. 14, 2022, Art. no. 1630.
- [8] L. Jakob and N. Gourmelen, “Glacier mass loss between 2010 and 2020 dominated by atmospheric forcing,” *Geophys. Res. Lett.*, vol. 50, 2023, Art. no. e2023GL102954.
- [9] E. Ciraci, I. Velicogna, and S. Swenson, “Continuity of the mass loss of the world’s glaciers and ice caps from the GRACE and GRACE follow-on missions,” *Geophys. Res. Lett.*, vol. 47, 2020, Art. no. e2019GL086926.
- [10] Q. Wang, S. Yi, and W. Sun, “Continuous estimates of glacier mass balance in high mountain Asia based on ICESat-1, 2 and GRACE/GRACE follow-on data,” *Geophys. Res. Lett.*, vol. 48, 2021, Art. no. e2020GL090954.
- [11] B. Wouters, A. S. Gardner, and G. Moholdt, “Global glacier mass loss during the GRACE satellite mission (2002–2016),” *Front. Earth Sci.*, vol. 7, pp. 1–11, 2019.
- [12] G. Zhang, T. Yao, H. Xie, S. Kang, and Y. Lei, “Increased mass over the Tibetan Plateau: From lakes or glaciers?,” *Geophys. Res. Lett.*, vol. 40, pp. 2125–2130, 2013.
- [13] IPCC, “Climate change– the physical science basis: Working Group I contribution to the sixth assessment report of the intergovernmental panel on climate change.” Geneva, Switzerland, 2021.
- [14] X. Xu, W. Wang, D. Huang, X. Hu, and W. Fu, “Assessment of interannual and seasonal glacier mass changes in the Karakoram during 2018–2022 using ICESat-2 data,” *J. Hydrol.*, vol. 626, 2023, Art. no. 130223.
- [15] B. Menounos, A. Gardner, C. Florentine, and A. Fountain, “Brief communication: Recent estimates of glacier mass loss for Western North America from laser altimetry,” *Cryosphere*, vol. 18, pp. 889–894, 2024.
- [16] J. Tong, Z. Shi, J. Jiao, B. Yang, and Z. Tian, “Glacier mass balance and its impact on land water storage in the Southeastern Tibetan plateau revealed by ICESat-2 and GRACE-FO,” *Remote Sens.*, vol. 16, 2024, Art. no. 1048.
- [17] K. Brunt, B. Smith, T. Sutterley, N. Kurtz, and T. Neumann, “Comparisons of satellite and airborne altimetry with ground-based data from the interior of the Antarctic ice sheet,” *Geophys. Res. Lett.*, vol. 48, Dec. 2021, Art. no. e2020GL090572.
- [18] X. Shen, C. Q. Ke, X. Yu, Y. Cai, and Y. Fan, “Evaluation of ice, cloud, and land elevation Satellite-2 (ICESat-2) land ice surface heights using airborne topographic mapper (ATM) data in Antarctica,” *Int. J. Remote Sens.*, vol. 42, pp. 2556–2573, 2021.
- [19] Y. Fan, C. Q. Ke, X. Zhou, X. Shen, X. Yu, and D. Lhakpa, “Glacier mass-balance estimates over high mountain Asia from 2000 to 2021 based on ICESat-2 and NASADEM,” *J. Glaciology*, vol. 69, pp. 500–512, 2023.
- [20] Q. Wang and W. Sun, “Seasonal cycles of high mountain Asia glacier surface elevation detected by ICESat-2,” *J. Geophys. Res., Atmos.*, vol. 127, 2022, Art. no. e2022JD037501.
- [21] B. Smith et al., “Land ice height-retrieval algorithm for NASA’s ICESat-2 photon-counting laser altimeter,” *Remote Sens. Environ.*, vol. 233, 2019, Art. no. 111352.
- [22] W. Chen et al., “Towards ice thickness inversion: An evaluation of global DEMs by ICESat-2 in the glacierized Tibetan Plateau,” *Cryosphere*, vol. 16, pp. 197–218, 2021.
- [23] T. Slater et al., “A new digital elevation model of Antarctica derived from CryoSat-2 altimetry,” *Cryosphere*, vol. 12, pp. 1551–1562, 2018.
- [24] R. McNabb, C. Nuth, A. Kääb, and L. Girod, “Sensitivity of glacier volume change estimation to DEM void interpolation,” *Cryosphere*, vol. 13, pp. 895–910, 2019.
- [25] Y. Zhou, Z. Li, J. Li, R. Zhao, and X. Ding, “Glacier mass balance in the Qinghai Tibet Plateau and its surroundings from the mid-1970s to 2000 based on Hexagon KH-9 and SRTM DEMs,” *Remote Sens. Environ.*, vol. 210, pp. 96–112, 2018.
- [26] K. K. Rosa, C. Perondi, B. K. Veettil, J. D. Auger, and J. C. Simões, “Contrasting responses of land-terminating glaciers to recent climate variations in King George Island,” *Antarctica Antarctic Sci.*, vol. 32, pp. 398–407, 2020.
- [27] C. Larsen, E. Burgess, A. Arendt, S. O’neil, A. Johnson, and C. Kienholz, “Surface melt dominates Alaska glacier mass balance,” *Geophys. Res. Lett.*, vol. 42, pp. 5902–5908, 2015.
- [28] A. Cremona, M. Huss, J. M. Landmann, J. Borner, and D. Farinotti, “European heat waves 2022: Contribution to extreme glacier melt in Switzerland inferred from automated ablation readings,” *Cryosphere*, vol. 17, pp. 1895–1912, 2023.
- [29] C. Xu, H. Li, F. Wang, Z. Li, P. Zhou, and S. Liu, “Heatwaves in summer 2022 forces substantial mass loss for Urumqi Glacier No. 1, China,” *J. Glaciology*, pp. 1–5, 2024.

Yubin Fan received the B.S. degree in geographic information science from Nanjing University of Posts and Telecommunications, Nanjing, China, in 2018, and the Ph.D. degree in geography from the School of Geography and Ocean Science, Nanjing University, Nanjing, China, in 2024.

He is currently a teacher with Chizhou University, Anhui, China. His research interests include remote sensing of cryosphere, and polar climate change.



Lanhua Luo received the B.S. degree in Human geography and urban and rural planning from Human Agricultural University, Changsha, China, in 2018, and the M.S. degree in cartography and geography information system from Nanjing Normal University, Nanjing, China, in 2021. She is currently working toward the Ph.D. degree in geography with the School of Geography and Ocean Science, Nanjing University, Nanjing.

Her research interests include remote sensing of cryosphere, climate change, and remote sensing image processing.





Chang-Qing Ke received the B.S. degree in geography from Shaanxi Normal University, Xi'an, China, in 1993, the M.S. degree in geography from the Lanzhou Institute of Glaciology and Geocryology, Chinese Academy of Sciences, Lanzhou, China, in 1996, and the Ph.D. degree in geography from the Nanjing Institute of Geography and Limnology, Chinese Academy of Sciences, Nanjing, China, in 1999.

From 1999 to 2002, he was a Postdoctoral Research Fellow with the School of Geography and Ocean Science, Nanjing University, Nanjing, where he has been an Associate Professor and a Full Professor in remote sensing since 2002 and 2007, respectively. His research interests include satellite image processing, remote sensing of cryosphere and water resource, and climate change.



Genyu Wang received the B.S. degree in geographical information science from Nanjing University, Nanjing, China, in 2019, and the M.S. degree in solid earth geophysics from National Institute of Natural Hazards, Beijing, China, in 2022. He is currently working toward the Ph.D. degree in geography with the School of Geography and Ocean Science, Nanjing University.

His research interests include remote sensing of snow and ice hydrology and climate change.